Crystalline Polymers in Nanoscale 1D Spatial Confinement

Ya-Sen Sun,[†] Tsai-Ming Chung,[‡] Yi-Jing Li,[‡] Rong-Ming Ho,*[,‡,§] Bao-Tsan Ko,[§] U-Ser Jeng,[†] and Bernard Lotz[||]

National Synchrotron Radiation Research Center, Hsinchu 30076 Taiwan, Department of Chemical Engineering, National Tsing-Hua University, Hisnchu 30013 Taiwan, Material and Chemical Research Laboratories, Industrial Technology Research Institute, Hsinchu 30013 Taiwan, and Institute Charles Sadron, 6 Rue Boussingault, Strasbourg 67083 France

Received April 11, 2006; Revised Manuscript Received June 12, 2006

ABSTRACT: A series of semicrystalline block copolymers, poly(4-vinylpyridine)-*block*-poly(ϵ-caprolactone) (P4VP−PCL), with lamellar microstructure have been synthesized. Owing to the vitrified P4VP microdomains and strongly segregated microphase separation, the crystallization of the PCL blocks in P4VP−PCL was carried out within the nanoscale confinement. Simply by varying the molecular weight of the block copolymer, namely the confined size, polymeric crystallization can be tailored in the one-dimensional confinement. A distinct nucleation mechanism, altering from heterogeneous to homogeneous nucleation, was obtained once the confined size became smaller than a critical dimension, equivalent to the regular thickness of heterogeneously nucleated crystalline lamellae. Consequently, discrete crystalline granules were generated through homogeneous nucleation, namely a single nucleus within one granule. Also, crystal growth was altered from specific to random orientation with respect to the interface between the crystalline and amorphous domains in the copolymers. This system thus serves as a model to analyze the impact of confined size in 1D spatial confinement on the crystallization of polymers.

Introduction

Recently, efforts have been dedicated to the physical properties of crystallizing materials in a confined space of a few nanometers or billionths of a meter because nanoscale confinement could be harnessed as a "synthetic tool" to create new properties and morphologies of materials for diverse applications.[1−3] Inorganic/organic templates with one-, two-, or three-dimensional confinements have been used to manipulate the crystallization of materials.[4−6] Crystal morphology and crystallization behavior significantly change, once the size of restricted geometries is comparable to the dimension of the crystallizing materials.

Full use of the templates to finely manipulate crystallization and thus crystalline properties in polymers remains a challenge. Self-assembled semicrystalline block copolymers (BCPs) possess inherently rich morphologies (for instance, lamellae, cylinders, spheres, and gyroids) on the nanometer scale.[7−9] They thus offer various nanoscale confined environments to tailor the crystallization kinetics of crystallizable blocks in BCPs.[7−31] However, an incorporation of crystallizable moiety within a BCP often adds morphological complexities due to the interplay among crystallization of the crystallizable block, microphase separation, and vitrification of the amorphous block. In other words, the final morphology of self-assembly semicrystalline BCPs is strongly dependent upon the experimental temperature, with respect to the order−disorder transition temperature (T_{ODT}), the crystallization temperature of the crystallizable block (T_c^c) and the glass transition temperature of amorphous block (T_g^a).[10−31] In crystalline systems with $T_{ODT} > T_g^a > T_c^c$ (that is a hard confinement for crystallization),[10,17−20] crystallization of a crystallizable block may occur within preexisting microdomains (MDs) created by microphase separation. In contrast, the morphology becomes more complicated when an amorphous block is rubbery during crystallization: the microphase-separated MDs can be preserved, templated, undulated, or even broken upon crystallization, depending on the segregation strength of microphase separation at the crystallization temperature (that is $(\chi N)_{Tc}$ where χN is the product of χ, the segmental interaction parameter, and N is the total number of segments in a block copolymer).[11−16,21−24] Extensive studies on the crystallization of polymers within discrete spherical and cylindrical MDs of asymmetric BCPs with strong incompatibility suggest that crystallization under nanoscale confinement might be initiated by homogeneous nucleation, different to the typical heterogeneous nucleation for homopolymers.[11−14] Nevertheless, the intrinsic crystallization behavior, in particular the nucleation mechanism, within lamellar MDs (namely, one-dimensional (1D) confined geometry) is still in debate.[13,16] On the other hand, the crystal orientation can be tailored by the control of the segregation strength[31] (upon varying molecular weight from medium to very weak segregation strength limits) or by crystallization temperature.[19] In this contribution, we focus on crystallization in lamellar-forming, semicrystalline BCPs with vitrified environments and strong segregation limits. A series of semicrystalline BCPs, poly(4-vinylpyridine)-*block*-poly(ϵ-caprolactone) (P4VP−PCL), with lamellar microstructure are synthesized. Owing to the "effective confinement" in the P4VP−PCL systems with a hard confinement ($T_{ODT} > T_g^a > T_c^c$) and strong segregation (high $(\chi N)_{Tc}$ value) for crystallization, the PCL crystallization is conducted between vitrified P4VP lamellar MDs. Consequently, polymeric crystallization can be tailored within the nanoscale MDs of BCPs. A transformation in nucleation mechanism of isothermal crystallization kinetics, from heterogeneous to homogeneous nucleation, with a decrease in the confined size, is identified due to the frustration of crystal

* To whom all correspondence should be addressed. Telephone: 886-3-573834. Fax: 886-3-5715408. E-mail: rmho@mx.nthu.edu.tw.
[†] National Synchrotron Radiation Research Center.
[‡] Department of Chemical Engineering, National Tsing-Hua University.
[§] Material and Chemical Research Laboratories, Industrial Technology Research Institute.
[||] Institute Charles Sadron.

10.1021/ma0608121 CCC: $33.50
Published on Web 07/19/2006

Scheme 1. Synthesis of P4VP−PCL Diblock Copolymers and PCL Homopolymers

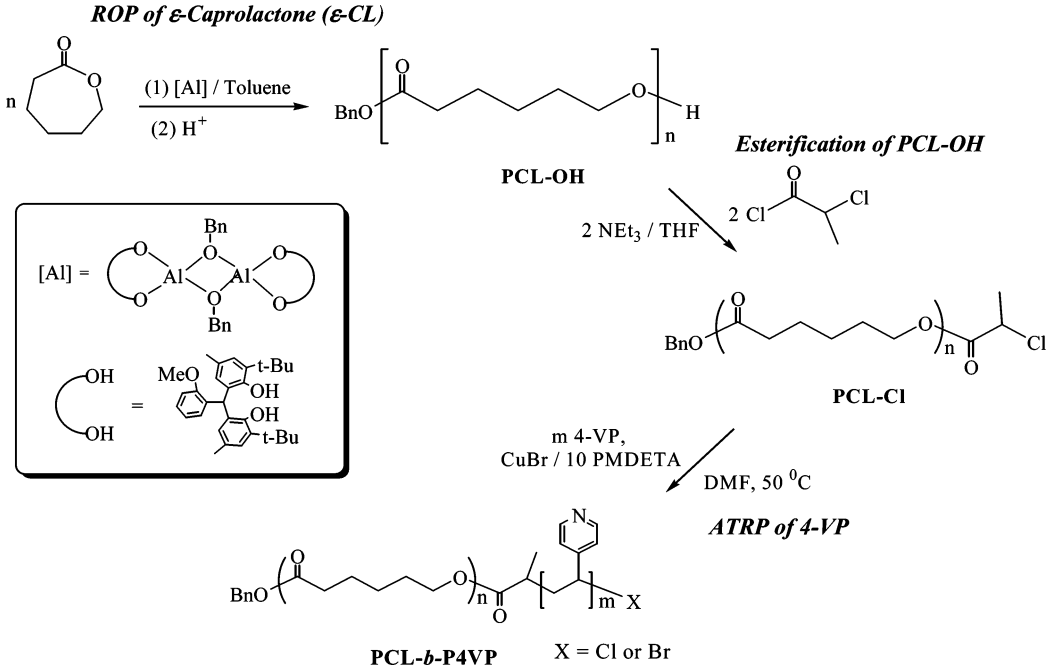

Table 1. Characterization of P4VP−PCL Diblock Copolymers and PCL Homopolymers

sample[a]	M_n^{total} (kg/mol)	M_n^{P4VP} (kg/mol)[b]	M_n^{PCL} (kg/mol)[b]	N_{total} [c]	M_w/M_n[d]	f_{PCL}[e]	morphology
VP/CL 47/46	10.4	5.0	5.4	93	1.27	0.50	lamellae
VP/CL 146/91	25.9	15.3	10.6	237	1.26	0.39	lamellae
VP/CL 69/46	12.7	7.3	5.4	115	1.20	0.40	lamellae
VP/CL 56/38	10.2	5.8	4.4	94	1.17	0.40	lamellae
VP/CL 42/25	7.3	4.4	2.9	67	1.17	0.37	lamellae
hCL 91	10.6				<1.1	1	
hCL 46	5.4				<1.1	1	
hCL 38	4.4				<1.1	1	
hCL 25	2.9				<1.1	1	

[a] VP/CL *m*/*n*, where *m* and *n* represent the degree of polymerization of the constituted P4VP (N_{P4VP}) and PCL (N_{PCL}) blocks, respectively. [b] M_n^{P4VP} and M_n^{PCL} were characterized by proton nuclear magnetic resonance (^{1}H NMR) and gel permeation chromatography (GPC). [c] $N_{total} = N_{P4VP} + N_{PCL}$. [d] Polydispersity index (PDI) in the final diblock copolymers was determined by GPC using standard calibration. [e] $f_{PCL} = N_{PCL}/(N_{P4VP} + N_{PCL})$.

growth. Granules, with a single nucleus each, are seen to be confined within the lamellar MDs. In addition, the crystal orientation was also discussed. This system thus serves as a model to analyze the impact of confined size in 1D spatial confinement on the crystallization of polymers.

Experimental Section

Synthesis of P4VP−PCL Diblock Copolymers and PCL Homopolymers. A series of semicrystalline BCPs, P4VP−PCL diblock polymers, were synthesized via living ring opening (ROP) and atom-transfer radical polymerization (ATRP) in sequence (Scheme 1).[32,33] Different molecular weights (MWs) with PCL volume fractions ranging from 0.37 to 0.4 were obtained. The first step was to prepare benzyl ester end-functionalized poly(caprolactone)s, PCL−OHs, resulting from ROP of ϵ-caprolactone monomers. Then a chloride-terminated PCL was prepared as a macroinitiator, further used for the controlled polymerization of 4-vinylpyridine. The P4VP−PCL BCPs were briefly designated as VP/CL *m*/*n* in which *m* and *n* represent the degree of polymerization of each constituted block, respectively. Besides this, to better determine the temperature dependence of χ, a symmetric VP/CL 47/46 was synthesized. The characterization of the resultant copolymers (P4VP−PCL) is tabulated in Table 1. For comparison, we synthesized four PCL "homopolymers" (labeled hCL *n*, in which *n* represents the degree of polymerization of PCL) having MWs similar to those of the corresponding PCL blocks in P4VP−PCL. Also, their characteristics are listed in Table 1.

Sample Preparation. To avoid grain boundaries and defects residing in microphase-separated P4VP−PCL samples, we achieved an oriented MD of BCPs on dissolving P4VP−PCL (10% by mass) in dichloromethane solution, followed by a novel rimming coating procedure outlined previously.[21] To eliminate possible effects of PCL crystallization and residual solvent on MDs during the rimming coating process, we annealed all oriented bulk samples at 140 °C for 12 h, which is above the glass transition temperature of P4VP blocks (T_g^{P4VP} = 130 °C) and well above the equilibrium melting point (T_m° = 69 °C) of PCL blocks, and then subjected samples to various thermal-annealing schemes under a nitrogen atmosphere.

Small-Angle X-ray Scattering (SAXS) and Wide-Angle X-ray Diffraction (WAXD). 2D SAXS/WAXD experiments were performed at BL01B SWLS beamline at the National Synchrotron Radiation Research Center (NSRRC), Taiwan. The incident X-ray beam was focused vertically by a mirror and monochromated to the energy of 10.5 keV by a germanium (111) double-crystal monochromator. The wavelength of the X-ray beam was λ = 1.18095 Å. The beam stop was a round tantalum disk 4 mm in diameter. The 2D SAXS/WAXD patterns were collected on Fuji plates using X-rays from a synchrotron. The scattering vectors, q ($q = (4\pi/\lambda) \times \sin(\theta/2)$, where θ is the scattering angle) in these patterns were calibrated using the two standard samples: silver behenate (SAXS) and α-Al_2O_3 (WAXD), respectively. Contribution of air scattering was subtracted from both the 2D SAXS and WAXD patterns. In situ SAXS experiments at various temperatures were carried out to determine the temperature dependence of χ, T_{ODT}, and χN of a series of block copolymers.

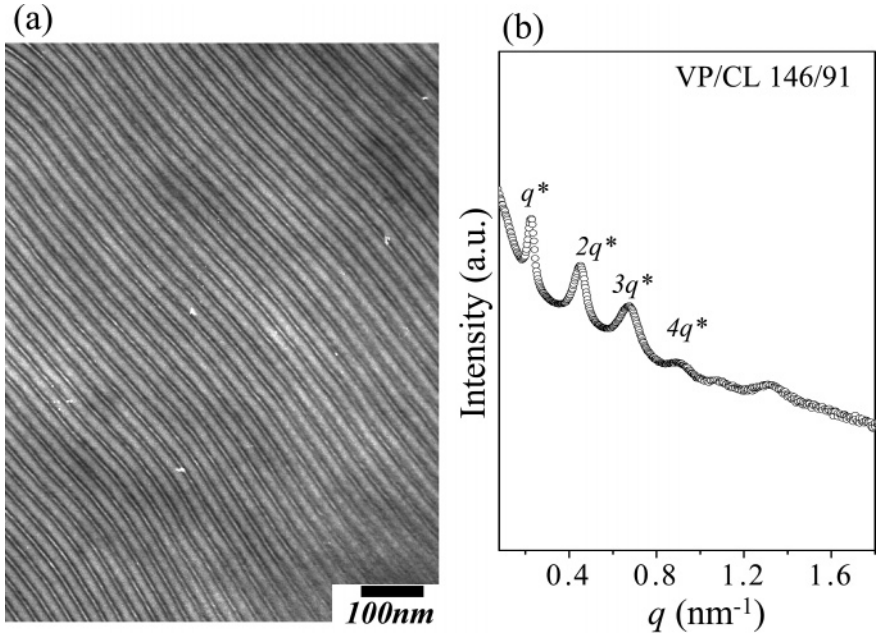

Figure 1. (a) TEM micrograph and (b) corresponding 1D SAXS profile of the VP/CL 146/91 at room temperature.

Differential Scanning Calorimeter (DSC). Nonisothermal and isothermal crystallization experiments of PCL blocks within the 1D confined lamellar MDs and PCL homopolymers were examined using a differential scanning calorimeter (DSC-7 Perkin-Elmer) equipped with a mechanical intracooler. The DSC instrument was properly calibrated with an indium standard at a scan rate of 10 °C/min. Samples were annealed at 80 °C for 5 min, by quenching to preset temperatures for isothermal crystallization; then, the scan rate of 10 °C/min was employed to record the endotherms of the PCL crystals in the P4VP−PCL BCPs and PCL homopolymers. For nonisothermal crystallization experiments, the crystallization exotherms, T_f, of the samples were recorded by a cooling rate of 10 °C/min from the melt at 80 °C.

Crystalline Lamellar Thickness Analysis. To visualize the crystalline PCL stems within the confined environment, the values of l_C were obtained from various PCL homopolymers having a variety of MWs. The morphological parameters of crystalline structures, such as long period (L), thickness of amorphous layers (l_a), and thickness of crystalline stems (l_C) were extracted from SAXS profiles via a one-dimensional correlation. Their thicknesses were deduced by the one-dimensional correlation function imposed on SAXS data after air scattering subtraction, followed by curve corrections for extrapolation of intensity to low q via the Debye−Bueche law and for extension to high q via the Porod's law. For the PCL homopolymers, the thicknesses of the crystalline stems ranging from 7 to 8 nm were found in the crystallization temperature region (10−45 °C), regardless of MW. Moreover, we found that relationships between T_m (measured from the peak temperature of endothermic response in DSC thermogram) and T_c for the PCL crystalline stems in BCPs and PCL homopolymers both obey the Hoffman−Weeks equation. Consequently, we presume that the crystals with a characteristic thickness (l_C) formed from an isothermal crystallization at a given T_c correspond well to a specific T_m in homopolymers and BCPs as well. Using the Gibbs−Thomson equation, the characteristic thickness of the crystalline PCL stems in BCPs were thus reasonably estimated from plots of inverse crystal lamellar thickness vs temperature from the evolution of the SAXS data of homopolymers.

Transmission Electron Microscopy (TEM). Prior to TEM characterization, the bulk P4VP−PCL samples were isothermally melt-crystallized in the DSC and then extracted from the DSC pans, followed by ultracryomicrotoming at −120 °C using a Reicher Ultracut microtome (equipped with a Reichert FCS cryochamber and a diamond knife). Staining was achieved by exposing the microtomed thin films to the vapors of a 4% aqueous RuO_4 solution for 30 min. A JEOL JEM-1200x transmission electron microscope was used (accelerating voltage: 120 kV).

Results and Discussion

Lamellar Morphology of P4VP—PCL with Various Molecular Weights. The microphase-separated microstructures of P4VP−PCL were examined with SAXS and TEM. Because of the RuO_4 staining, the P4VP MDs are dark and the PCL MDs appear light. As expected from the composition, a lamellar microstructure was observed at room temperature for the quenched VP/CL 146/91 sample (Figure 1a). The corresponding SAXS result for the VP/CL 146/91 sample at room temperature further confirms the observed lamellar microstructure, with the scattering peaks being at q ratio of 1:2:3:4 (Figure 1b). However, the peaks are broadened but keep essentially the same positions as in the melt, indicating that the lamellar morphology is essentially preserved after crystallization. The peak broadening may result from the fact that after PCL block crystallization the electron density within the PCL domains is less uniform than in the melt. The additional heterogeneity is created by PCL crystallites within the assembled PCL lamellar MDs. The breadths of the peaks become narrow at temperatures above the T_m of PCL blocks, as illustrated in Figure 2, for which the 1D SAXS profiles were recorded at 80 °C to eliminate the PCL crystallites. Similar morphological results were also obtained for other three P4VP−PCL BCPs with different MWs. The SAXS results yield long periods of microphase-separated lamellae according to an expression $d_{lam} = 2\pi/q^*$ in which q^* is the position of the principal feature. Combining the long periods and the volume fractions of PCL blocks (f_{PCL}^{v}), the PCL lamellae (d_{PCL}) are approximately 4.7 (VP/CL 42/25), 6 (VP/CL 56/38), 8.8 (VP/CL 69/46), and 11 nm (VP/CL 146/91) therein, respectively. As a result, the microphase-separated lamellae having various long periods can be obtained upon varying the MW of the BCP.

Strong Segregated Microphase Separation. To determine the segregation strength of microphase separation, temperature-resolved SAXS measurements were employed for determining T_{ODT} so as to calculate the χ value of the synthesized BCPs.[34] Nevertheless, thermal degradation occurs once temperature is above 200 °C, as evidenced by thermal gravimetric analysis

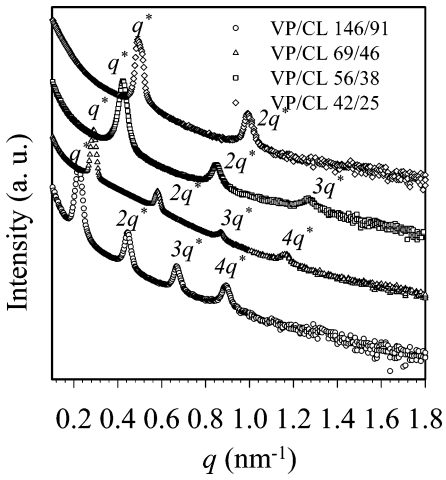

Figure 2. 1D SAXS profiles of VP/CL copolymers at 80 °C.

(TGA). Even so, these BCPs are expected not to disorder up to the decomposition point (>200 °C) on the basis of the in situ SAXS results. Instead, the measurement of χ is evaluated according to the characteristic domain spacing, $d_{lam} = 1.10aN^{2/3}\chi^{1/6}$, for a symmetric diblock copolymer with the lamellar MD in strong segregation limits.[35] a is the average statistical segment length and χ the temperature-dependent interaction parameter.

A symmetric VP/CL 47/46 ($f_{CL}^{v} = 0.5$) was served to determine the temperature dependence of χ value. The average statistic segment length for the VP/CL 47/46 was calculated by $a_{VP/CL} = (f_{VP}^{v}/a_{VP}^{2}+f_{CL}^{v}/a_{CL}^{2})^{-1/2}$ at which $f_{VP}^{v} = 0.5$ and $f_{CL}^{v} = 0.5$ are volume fraction of each block with the statistical segments of $a_{VP} = 7.4$ Å and $a_{CL} = 9.6$ Å,[36] respectively. By measuring the characteristic domain spacing (d_{lam}) from temperature-resolved SAXS results (as shown in Figure 3), the temperature dependence of χ can be determined. A plot of χ vs $1/T$ is described with $\chi(T) = 103.48/T - 0.062$. On the basis of self-consistent field theory for a symmetric diblock copolymer,[9,34] the estimated T_{ODT} values of the P4VP−PCL synthesized are far above 200 °C, consistent with the experimental observations. Figure 4 demonstrates the MW dependence of the long periods is consistent with the expected scaling law of the strong segregation limits[34,35] ($d_{total} \sim N^{0.652}$) and PCL domains as well ($d_{PCL} \sim N^{0.676}$). It is also noted that the amorphous P4VP matrix has a glass transition temperature of 130 °C, which is much higher than the melting point of PCL crystallites (i.e., hard confinement). Consequently, a well-defined system with strong segregation limits (high $(\chi N)_{T_c}$ value) for polymer crystallization under vitrified nanoscale confinement was generated. Subsequent nonisothermal/isothermal crystallization of the P4VP−PCLs indicates that the principal features and the diffraction positions of the SAXS profiles are almost identical to amorphous P4VP−PCLs, revealing that the lamellar microstructure is faithfully preserved after crystallization.

Confined Size Effect. Nonisothermal crystallization experiments were first employed to examine the maximum crystallization-rate-temperature (T_f) during cooling. Figure 5 indicates only a slight dependence of T_f on the MW of PCL homopolymers. This suggests that the effect of MW on nonisothermal crystallization kinetics is negligible. By contrast, we found a significant variation of T_f of PCL block crystallized in confined lamellae because of the confinement effect. The T_f of the PCL block is usually lower than that of homopolymer. However, a much more significant decrease of T_f was observed when the dimension of the confined size became less than 8 nm. For a 4.7 nm dimension, PCL component even cannot crystallize upon

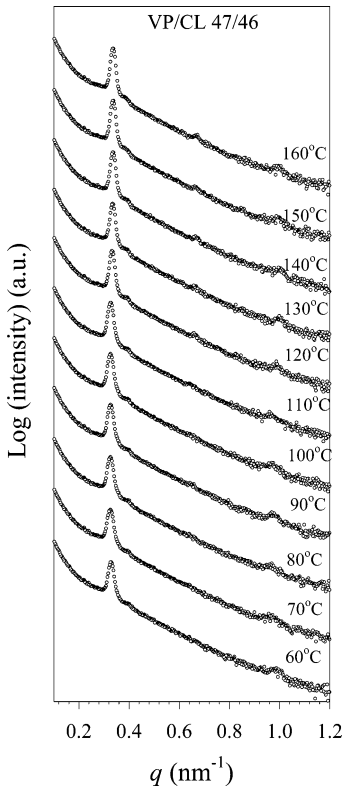

Figure 3. Set of SAXS curves of the VP/CL 47/46 at various temperatures. Noted, the temperature dependence of $\chi_{VP/CL}$ for VP/CL 47/46 tested here was determined from SAXS profiles at various temperatures above 120 °C to avoid nonequilibrium effects below the glass transition temperature of P4VP.

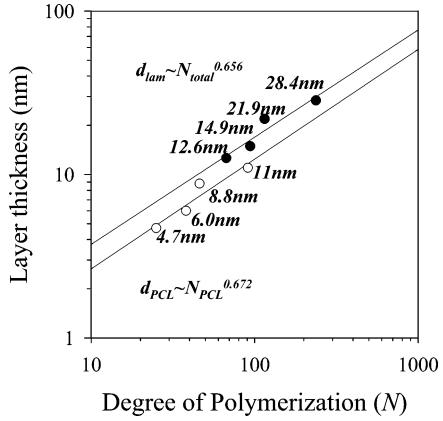

Figure 4. Two log−log plots of d_{lam} and d_{PCL} as a function of $N_{overall}$ and N_{PCL} for different MW, in which d_{lam} and d_{PCL} were evaluated from the SAXS patterns collected at 80 °C.

cooling. As a result, the confined size really matters for crystallization under confinement. Notably, the confinement retards profoundly the polymer crystallization once the confined space is smaller than a dimension at the intersection of two log−log plots of d_{PCL} and l_C^{PCL} as a function of N_{PCL}. The dimension seems to represent a probable thickness, relevant to the crystalline lamellar thickness of homopolymers in typical crystallization temperature regions (10−45 °C).

Transformation from Heterogeneous to Homogeneous Nucleation. A large undercooling required to induce crystallization within the 6 nm confined lamellar space reflects the possible change in crystallization kinetics, in particular the nucleation process.[11−16] Isothermal crystallization is satisfactorily described with the Avrami equation by $X_C(t) = 1 - \exp(-Kt^n)$ where $X_C(t)$ is the normalized degree of crystallinity that

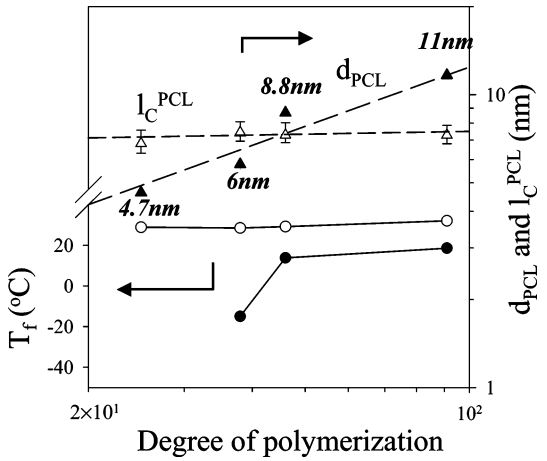

Figure 5. The log−log plots of d_{PCL} (solid triangles) and crystalline PCL stem thickness, l_C^{PCL}, (open triangles) as a function of N_{PCL} for different MWs and two plots of T_f vs logarithmic N_{PCL} of PCL blocks (solid circles) and PCL homopolymers (open circles).

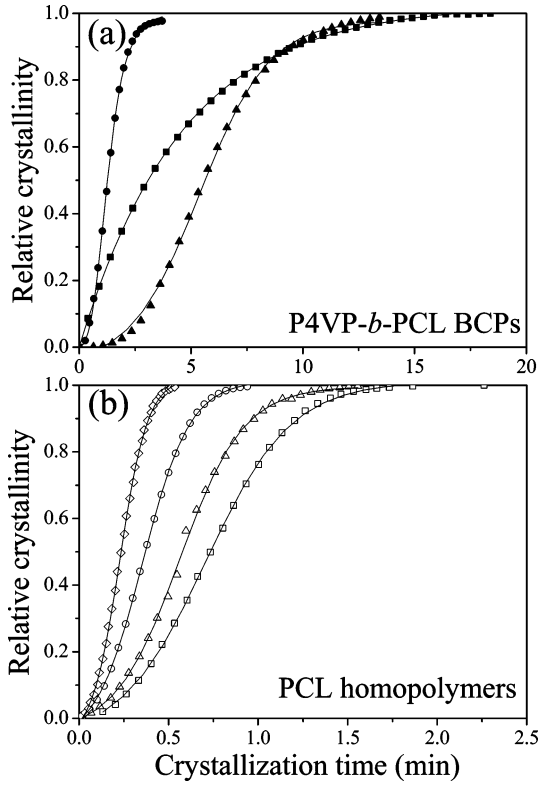

Figure 6. Development of crystallinity during isothermal crystallization at 30 °C in (a) P4VP−PCL BCPs and (b) PCL homopolymers: VP/CL 146/91 (solid circles), VP/CL 69/46 (solid triangles), hCL 91 (open circles), hCL 46 (open triangles), hCL 38 (open squares) and hCL 25 (open rhombi). It is noted, for VP/CL 56/38, that the development of crystallinity was measured upon crystallization at −20 °C (solid squares). The relative crystallinity was deduced from the enthalpy change during dynamic isothermal crystallization in a DSC.

has formed at time t, and the prefactor K and exponent n are Avrami parameters.[12] As shown in Figure 6 a, the curve of exothermic response with duration of crystallization exhibits a simple exponential shape prescribed by first-order kinetics (i.e., a typical Avrami index $n = 1$)[12] for a confined lamellae size 6 nm, suggesting homogeneous nucleation. In contrast, in the case of BCPs with a larger confined size—either 8.8 or 11 nm, crystallization within lamellar MDs reveals a sigmoidal curve prescribed by Avrami exponent values greater than unity, reflecting that crystallization begins generally from heterogeneous nucleation followed by a long-range (typically micrometer-range) growth of a bundle of crystalline lamellae.[37−39] This sigmoidal shape was also observed for PCL homopolymers with general crystallization proceeding through heterogeneous nucleation and spherulitic growth (Figure 6b).

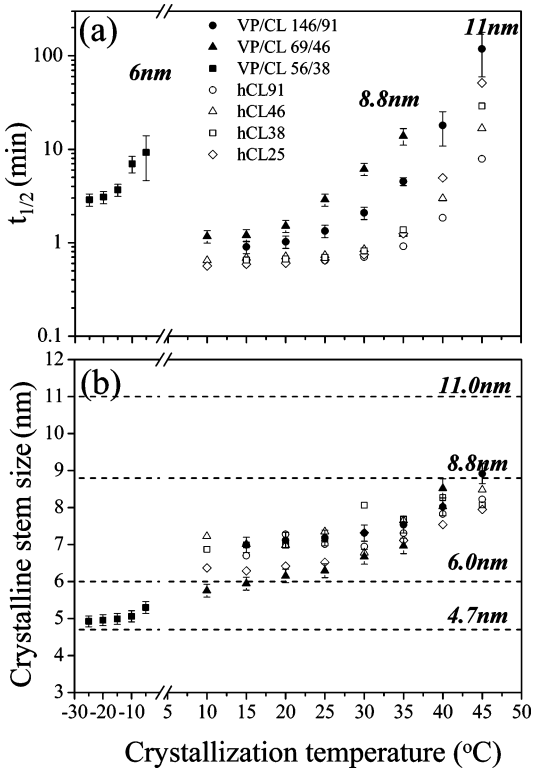

Figure 7. (a) Dependence of half-time of isothermal crystallization on temperature and (b) lamellar thickness, l_C^{PCL}, of crystalline PCL stems as a function of T_c for P4VP−PCL BCPs and PCL homopolymers. Horizontal lines denote the confined sizes. The characteristic thicknesses of crystalline PCL stems for BCPs were estimated from plots of inverse crystal lamellar thickness vs melting temperature from evolution of SAXS data.

The dependence of crystallization halftime ($t_{1/2}$) on T_c and d_{PCL} (i.e., confined size) was further examined. In Figure 7 a, the upward shift of $t_{1/2}(T_c)$ upon decreasing d_{PCL} from 11 (VP/CL 146/91) to 8.8 nm (VP/CL 69/46) reflects a significant effect of confined size on the rate of crystallization. Moreover, for high crystallization temperatures this effect becomes more pronounced when compared to the corresponding homopolymer having the same MW. Generally, crystallization at high temperatures, close to $T_m°$ of the PCL crystals, favors the growth of thicker crystalline stems with less chain folding. However, we speculate that this process is limited by the energetic barriers arising from the existing confinement.[40,41] Furthermore, the $t_{1/2}(T_c)$ curve of polymer crystallization shifted significantly to lower temperature when the confined size is decreased to 6 nm, for which the thickness of crystalline PCL stems is decreased to ∼5 nm, as evidenced in Figure 7b. A large undercooling is thus required to form the thin crystalline stems upon homogeneous nucleation, once the confined size becomes smaller than the thickness (7−8 nm) of the heterogeneous nucleation-tailored crystalline stem in the conventional crystallization range (10−45 °C). As many nucleation sites are created at lower T_c, the primary nucleation density is very high; hence little crystal-growth is needed to complete crystallization and random crystalline orientation is obtained.[18−19]

Tailored Crystalline Morphology Under Confinement. Results of TEM experiments and 2D SAXS/WAXD patterns,

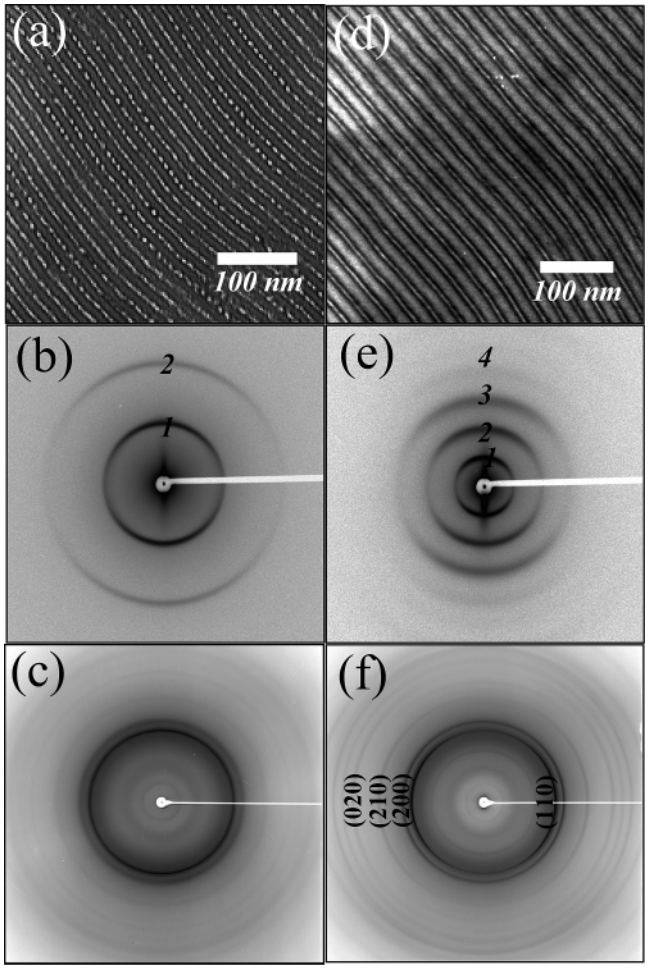

Figure 8. (a) TEM image of a thin section of oriented VP/CL 56/38 after PCL crystallization at −10 °C within self-assembled lamellae of size 6 nm stained with RuO_4, in which discrete spherelike granules and a necklace-like morphology (strings of beads) are identifiable; these necklace-like morphologies might result from overlapping discrete spherelike granules in projection. 2D anisotropic SAXS (b) and powder-ringed WAXD (c) patterns with X-ray beams along the X-direction (shear direction). (d) TEM image of a thin section of oriented VP/CL 146/91 after crystallization at 20 °C. The MDs of P4VP are dark (stained with RuO_4), whereas MDs of PCL are light. (e) 2D anisotropic SAXS and (f) fiberlike WAXD patterns with X-ray beams along the X-direction.

shown in Figure 8, parts a−c, confirm the hypothesis of homogeneous nucleation-tailored overall kinetics of crystallization. Close scrutiny of the TEM image (Figure 8a) indicates that the PCL crystalline regions are present as discrete single granules. Each single granule has one nucleus of thickness approximately 5 nm. Crystallization within such discrete spherelike granules is analogous to homogeneous nucleation of poly(ethylene oxide) (PEO) confined to the spherical MDs of highly asymmetric BCPs.[11−14,25] If we assume that the diameter of each spherical-like granule is about 6 nm in diameter, the nucleation density ($N\rho$) would be ca. 3.5×10^{18} nuclei/cm^3 (according to $N\rho = f_{PCL}{}^{v}/V_S{}^{PCL}$, in which $V_S{}^{PCL}$ is the average volume of an isolated granule). This very high nucleation density, which far exceeds the heterogeneous nucleation density typically found in homopolymers, makes homogeneous nucleation the rate-determining process.

By contrast, the single slab PCL crystals observed in Figure 8d differ remarkably from discrete granules, indicating that upon varying the confined size the dimensions of crystallites can be tailored by nucleation processes. The observed morphology demonstrates that the crystal growth starting from the heterogeneous nucleus can spread over the scale of a few tens of micrometers along the lamellar MDs with a confined size greater than 8 nm, which is in line with the interpretation based on the sigmoidal crystallization kinetics. In contrast to the random orientation with respect to the interface between the crystalline and amorphous domains in the copolymers (Figure 8, parts b and c) for the crystal growth of homogeneous nucleation, such a large confined space (e.g., 11 nm) allows perpendicular orientation of the crystalline PCL stems (Figure 8, parts e and f). The observed WAXD reflections were indexed by an orthorhombic unit cell with dimensions $a = 0.7096$ nm, $b = 0.4974$ nm, and $c = 1.7297$ nm.[42−43]

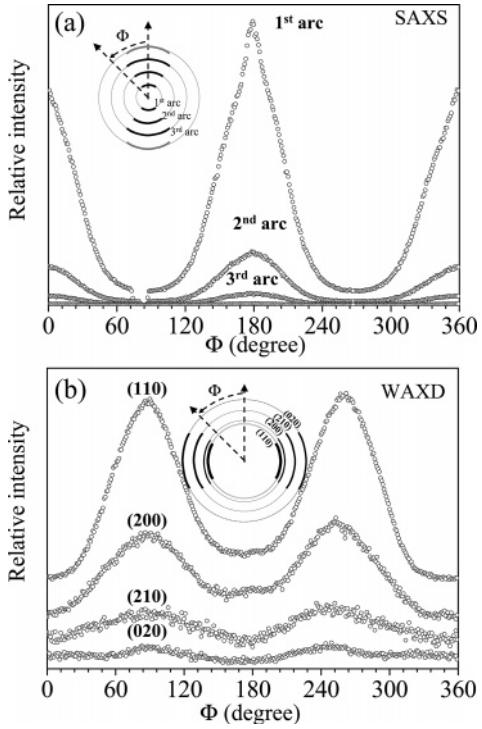

Figure 9. (a) Azimuthal profiles for the 2D SAXS pattern in Figure 8e. (b) Azimuthal profiles for the 2D WAXD pattern in Figure 8f.

To further confirm the aligned results, the azimuthal profiles of both the SAXS and WAXD patterns for VP/CL 146/91 melt-crystallized at 20 °C are obtained and plotted in Figure 9, parts a and b, respectively. For the SAXS pattern shown in Figure 9 a, the maximum intensities of all the observed scatterings locate at the azimuthal angle, $\Phi = 0$ and 180°. As for the WAXD patterns shown in Figure 9b, the maximum intensities of all the observed reflections locate at the azimuthal angle, $\Phi = 90$ and 270°. As a result, we conclude that a perpendicular orientation was found in the samples crystallized at high temperatures.

Figure 10 shows that upon varying the confined size, not only does a heterogeneous to homogeneous transition occur, but the dimensions of crystallites can also be tailored by nucleation processes. For the confined space >8 nm, the heterogeneous nucleation typically occurs at shallow undercooling. The PCL crystalline stems are normal to the domain wall so as to allow two-dimensional crystal growth along the $X-Y$ plane.[26−31] In contrast, for the confined space <8 nm, the homogeneous nucleation occurs at extremely deep undercooling. The extent of crystal growth is only governed by the size of spatial confinement, and crystal growth throughout an entire microdomain is essentially instantaneous once nucleation occurs. Therefore, the crystallization within the 6 nm lamellae proceeds via a homogeneous nucleation regardless of the lateral length

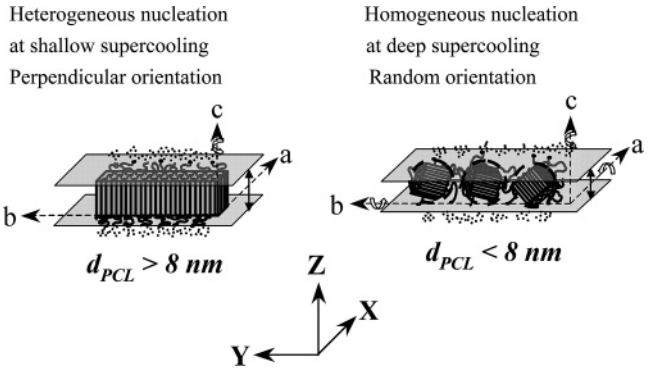

Figure 10. Left: probable structure of the slab crystalline PCL stem. Right: spherelike crystalline PCL stems. Dotted circles illustrate possible granules self-created through homogeneous nucleation.

of the confined lamellae. As a result, random crystalline orientation (zero-dimensional crystal growth) was prevailing for each tiny granule formed by one nucleation event through homogeneous nucleation.

We now examine how the crystallization of PCL becomes substantially hindered when the confined gap is 4.7 nm. As mentioned, an extremely low T_c is required to initiate polymer crystallization in the 4.7 nm confined lamellae in order to overcome the intrinsic barrier for homogeneous nucleation.[44,45] However, approaching the glass transition temperature, $T_g^{PCL} = -69$ °C, of PCL block decreases the chain mobility so that forming a nucleus becomes extremely difficult. Moreover, the probability of homogeneous nucleation depends directly on the volume of materials. For a small confining space 4.7 nm, the overall crystallization kinetics via homogeneous nucleation would be much slower than for the 6 nm confining space so that the crystalline block becomes noncrystallizable on the ordinary time scale allowed for crystallization.

Conclusion

In summary, we have shown that the tuning of confined size afforded by changing the molecular parameters provides an effective approach to finely tailor the polymer crystallization and morphology in the lamellar-forming BCPs. The effective confinement allows not only the change of nucleation mechanism from heterogeneous to homogeneous nucleation but also the transformation in crystallographic orientation from perpendicular to random type. Even the crystallizable block inside the smallest space studied may be unable to crystallize. The dependence of polymer crystallization behavior on confined size may be extended to explore some fundamental aspects of crystal nucleation and growth, and develop strategies to the control of nanostructures and the anisotropic properties of crystallizing materials under nanoscale 1D confinement.

Acknowledgment. We thank the National Science Council for support (NSC-93-2216-E−007-010). The SAXS experiments were conducted at beamline BL01B at the National Synchrotron Radiation Research Center (NSRRC), Taiwan.

References and Notes

(1) Thurn-Albrecht, T.; Schotter, J.; Kästle, G. A.; Emley, N.; Shibauchi, T.; Krusin-Elbaum, L.; Guarini, K.; Black, C. T.; Tuominen, M. T.; Russell, T. P. *Science* **2000**, *290*, 2126.
(2) Shin, K.; Xiang, H.; Moon, S. I.; Kim, T.; McCarthy, T. J.; Russell, T. P. *Science* **2004**, *306*, 76.
(3) Huck, W. T. S. *Chem. Commun.* **2005**, *33*, 4143.
(4) Ha, J. M.; Wolf, J. H.; Hillmyer, M. A.; Ward, M. D. *J. Am. Chem. Soc.* **2004**, *126*, 3382.
(5) Wu, Y.; Cheng, G.; Katsov, K.; Sides, S. W.; Wang, J.; Tang, J.; Fredrickson, G. H.; Moskovits, M.; Stucky, G. D. *Nat. Mater.* **2004**, *3*, 816.
(6) Zhang, Q.; Wang, M.; Wooley, K. L. *Curr. Org. Chem.* **2005**, *9*, 1053.
(7) Bates, F. S.; Fredrickson, G. H. *Phys. Today* **1999**, *52*, 32.
(8) Bates, F. S.; Fredrickson, G. H. *Annu. Rev. Phys. Chem.* **1990**, *41*, 525.
(9) Hamley, I. W. In *The Physics of Block Copolymers*; Oxford University Press: New York, 1998, Chapter 5 and references therein.
(10) Lotz, B.; Kovacs, A. J. *ACS Polym. Prepr.* **1969**, *10*, 820.
(11) Loo, Y.-L.; Register, R. A.; Ryan, A. J. *Macromolecules* **2002**, *35*, 2365.
(12) Loo, Y.-L.; Register, R. A.; Ryan, A. J. *Phys. Rev. Lett.* **2000**, *84*, 4120.
(13) Loo, Y.-L.; Register, R. A.; Ryan, A. J.; Dee, G. T. *Macromolecules* **2001**, *34*, 8968.
(14) Loo, Y.-L.; Register, R. A.; Adamson, D. H. *Macromolecules* **2000**, *33*, 8361.
(15) Chen, H. L.; Hsiao, S. C.; Lin, T. L.; Yamauchi, K.; Hasegawa, H.; Hashimoto, T. *Macromolecules* **2001**, *34*, 671.
(16) Chen, H. L.; Wu, J. C.; Lin, T. L.; Lin, J. S. *Macromolecules* **2001**, *34*, 6936.
(17) Huang, P.; Zhu, L.; Gau, Y.; Ge, Q.; Jing, A. J.; Chen, W. Y.; Quirk, R. P.; Cheng, S. Z. D.; Thomas, E. L.; Lotz, B.; Hsiao, B. S.; Avila-Orta, C. A.; Sics, I. *Macromolecules* **2004**, *37*, 3689.
(18) Zhu, L.; Cheng, S. Z. D.; Calhoun, B. H.; Ge, Q.; Quirk, R. P.; Thomas, E. L.; Lotz, B.; Hsiao, B. S.; Yeh, F.; Liu, L. *Macromolecules* **2001**, *34*, 1244.
(19) Zhu, L.; Cheng, S. Z. D.; Calhoun, B. H.; Ge, Q.; Quirk, R. P.; Thomas, E. L.; Hsiao, B. S.; Yeh, F.; Lotz, B. *J. Am. Chem. Soc.* **2000**, *122*, 5957.
(20) Zhu, L.; Cheng, S. Z. D.; Huang, P.; Ge, Q.; Quirk, R. P.; Thomas, E. L.; Lotz, B.; Hsiao, B. S.; Yeh, F.; Liu, L. *Adv. Mater.* **2002**, *14*, 31.
(21) Ho, R.-M.; Lin, F.-H. Tsai, C.-C.; Lin, C.-C.; Ko, B.-T.; Hsiao, B. S.; Sics, I. *Macromolecules* **2004**, *37*, 5985.
(22) Ho, R.-M.; Chung, T.-M.; Tsai, J.-C.; Kuo, J.-C.; Hsiao, B. S.; Sics, I. *Macromol. Rapid Commun.* **2005**, *26*, 107.
(23) Ho, R.-M.; Chiang, Y.-W.; Lin, C.-C.; Huang, B.-H. *Macromolecules* **2005**, *38*, 4769.
(24) Chung, T.-M.; Ho, R.-M.; Kuo, J.-C.; Tsai, J.-C.; Hsiao, B. S.; Sics, I. *Macromolecules* **2006**, *39*, 2739.
(25) Reiter, G.; Castelein, G.; Sommer, J. U.; Röttele, A.; Thurn-Albrecht, T. *Phys. Rev. Lett.* **2001**, *87*, 226101.
(26) Cohen, R. E.; Bellare, A.; Drzewinski, M. A. *Macromolecules* **1994**, *27*, 2321.
(27) Douzinas, K. C.; Cohen, R. E.; Halasa, A. F. *Macromolecules* **1991**, *24*, 4457.
(28) Douzinas, K. C.; Cohen, R. E. *Macromolecules* **1992**, *25*, 5030.
(29) Hamley, I. W.; Fairclough, J. P. A.; Terrill, N. J.; Ryan, A. J.; Lipic, P. M.; Bates, F. S.; Towns-Andrews, E. *Macromolecules* **1996**, *29*, 8835.
(30) Ryan, A. J.; Hamley, I. W.; Bras, W.; Bates, F. S. *Macromolecules* **1995**, *28*, 3860.
(31) Koo, C. M.; Wu, L.; Lim, L. S.; Mahanthappa, M. K.; Hillmyer, M. A.; Bates, F. S. *Macromolecules* **2005**, *38*, 6090.
(32) Ko, B. T.; Lin, C. C. *Macromolecules* **1999**, *32*, 8296.
(33) Xia, J.; Zhang, X.; Matyjaszewski, K. *Macromolecules* **1999**, *32*, 3531.
(34) Matsen, M. W.; Bates, F. S. *Macromolecules* **1996**, *29*, 1091.
(35) Semenov, A. N. *Sov. Phys. JETP* **1985**, *61*, 733.
(36) Brandrup, J.; Immergut, E. H. *Polymer Handbook*; Wiley: New York **1989.**
(37) Müller, A. J.; Albuerne, J.; Marquez, L.; Raquez, J. M.; Degée, P.; Dubois, P.; Hobbs, J.; Hamley, I. W. *Faraday Discuss.* **2005**, *128*, 231.
(38) Müller, A. J.; Albuerne, J.; Esteves, L. M.; Marquez, L.; Raquez, J. M.; Degée, P.; Dubois, P.; Collins, S.; Hamley, I. W. *Macromol. Symp.* **2004**, *215*, 369.
(39) Müller, A. J.; Balsamo, V. M.; Arnal, L.; Jakob, T.; Schmalz, H.; Abetz, V. *Macromolecules* **2002**, *35*, 3048.
(40) Chen, W. Y.; Zheng, J. X.; Cheng, S. Z. D.; Li, C. Y.; Huang, P.; Zhu, L.; Xiong, H.; Ge, Q.; Guo, Y.; Quirk, R. P.; Lotz, B.; Deng, L.; Wu, C.; Thomas, E. L. *Phys. Rev. Lett.* **2004**, *93*, 028301.
(41) Zheng, J. X.; Xiong, H.; Chen, W. Y.; Lee, K.; Van Horn, R. M.; Quirk, R. P.; Lotz, B.; Thomas, E. L.; Shi, A.-C.; Cheng, S. Z. D. *Macromolecules* **2006**, *39*, 641.
(42) Hu, H.; Dorset, D. L. *Macromolecules* **1990**, *23*, 4604.
(43) Bittiger, H.; Marchessault, R. H. *Acta Crystallogr.* **1970**, *B26*, 1923.
(44) Massa, M. V.; Carvalho, J. L.; Dalnoki-Veress, K. *Eur. Phys. J. E* **2003**, *12*, 111.
(45) Massa, M. V.; Dalnoki-Veress, K. *Phys. Rev. Lett.* **2004**, *92*, 255509.

MA0608121